Single-shot generation of a sonogram by time gating of a spectrally decomposed ultrashort laser pulse

Dmitriy Panasenko, Pang-Chen Sun, Nikola Alic, and Yeshaiahu Fainman

An experimental technique for single-shot generation of the sonogram of an ultrashort laser pulse is demonstrated. The method is based on the time gating of a spectrally decomposed test signal, transferring its spectral phase into a spatial phase, and the spatial filtering of the signal to produce a sonogram. The technique is evaluated experimentally, producing sonograms for linearly and nonlinearly chirped femtosecond laser pulses. The single-shot technique permits reconstruction of ultrashort pulse complex amplitude profiles and is useful for showing the signal in real time. © 2002 Optical Society of America

OCIS codes: 320.0320, 190.7110, 320.7100, 070.0070.

1. Introduction

Numerous applications of ultrashort-pulse lasers require characterization of the complex amplitude (i.e., the amplitude and the phase) of an ultrafast optical waveform. Time–frequency distributions such as spectrogram and sonogram have proved to be useful in answering this need, and various time–frequency techniques for detection of ultrashort laser pulses have been developed.[1–5] An important advantage of these techniques is that the time–frequency distribution gives intuitive insight into the properties of the complex signal. This advantage is fully realized in a single-shot acquisition system, which permits the ultrashort waveform to be shown in real time.

The most commonly used time–frequency technique is frequency-resolved optical gating (FROG),[1,2] which utilizes a spectrogram generated by detection of the power spectrum of a time-gated pulse. Time gating can be achieved by use of either a second- or a third-order nonlinear process. When third-order nonlinearity is used, the FROG trace is highly intuitive and directly displays simple phase distortions such as linear chirp.[1] However, third-order nonlinear effects require high laser power and in most cases can be used only with amplified femtosecond systems. A FROG trace generated with a second-order nonlinear process is insensitive to the sign of the chirp and gives less insight into the properties of the signal than is provided by third-order nonlinearity FROG before a computationally intensive iterative reconstruction algorithm is applied.[2]

An alternative time–frequency approach to detection of ultrashort pulses uses a sonogram, which is generated by measurement of the relative delays of various frequency components of the pulse under test.[3–5] A sonogram trace is sensitive to the sign of the chirp, as it directly displays the group delay of the signal that is analyzed. Experimentally, a sonogram can be obtained by use of second-order nonlinear processes and therefore can be used to analyze low-energy ultrashort pulses. Additionally, for a variety of practically important cases the complex amplitude of the optical signal can be extracted with a simple and fast noniterative algorithm. For single-shot operation, a time-domain technique based on wave mixing of the signal pulse with a spectrally filtered reference pulse has been developed.[4] In this paper we introduce an alternative technique for spectral-domain single-shot operation based on wave mixing of a spectrally decomposed signal with a time-domain gating pulse. Spectral decomposition followed by time gating converts the spectral phase of the test pulse into the spatial phase of a spectrally decomposed field. Further optical processing of the spatial wave front produces a single-shot sonogram trace.

Our paper is organized as follows: In Section 2 we review the algorithm that is used for reconstruction of the complex amplitude from the sonogram. In

D. Panasenko (dpanasen@ece.ucsd.edu), P.-C. Sun, N. Alic, and Y. Fainman are with the Department of Electrical and Computer Engineering, University of California San Diego, 9500 Gilman Drive, La Jolla, California 92093-0407.

Received 27 September 2001; revised manuscript received 21 March 2002.

0003-6935/02/245185-06$15.00/0

Section 3 we introduce and describe our technique for generating the sonogram; the experimental apparatus and the experimental results are presented in Section 4. The effect of gating pulse width on the measurements is analyzed in Section 5, followed by our conclusions in Section 6.

2. Complex Amplitude Reconstruction with the Sonogram

Consider an optical signal with complex amplitude $s(t)$ and its corresponding Fourier transform:

$$\tilde{s}(\nu) = \int s(t)\exp(-i2\pi\nu t)\mathrm{d}t, \tag{1}$$

where t and ν are time and frequency coordinates, respectively. The sonogram is defined as

$$W(t, \nu) = \left| \int \tilde{s}(\nu')G(\nu - \nu')\exp(-i2\pi\nu' t)\mathrm{d}\nu' \right|^2, \tag{2}$$

where $G(\nu)$ is a window function in the frequency domain. The sonogram has a simple physical interpretation: It shows the time at which the particular frequency components that have been selected by filter $G(\nu)$ appear in the signal. Similarly, a spectrogram defined in the time domain,[6]

$$\hat{W}(t, \nu) = \left| \int s(t')\hat{G}(t - t')\exp(i2\pi\nu t')\mathrm{d}t' \right|^2, \tag{3}$$

shows a frequency content that occurs in the signal within a time interval selected by filter $\hat{G}(t)$. Although the sonogram and the spectrogram are equivalent time–frequency signal representations [provided that filter functions $G(\nu)$ and $\hat{G}(t)$ are a Fourier-transform pair], they are generated in the frequency and the time domains, respectively, and for ultrashort pulse diagnostics it is useful to distinguish between the corresponding techniques. A time-domain spectrogram filter $\hat{G}(t)$ is usually derived from the ultrashort pulse signal itself[1]; therefore its duration is approximately equal to the duration of the pulse under test. In contrast, it is easy to achieve frequency-domain filter $G(\nu)$ with a bandwidth much narrower than that of the signal to be analyzed. In many cases this property of sonogram window function $G(\nu)$ permits the extraction of signal $s(t)$ by use of a simple noniterative algorithm, based on approximation of the spectral phase within filter $G(\nu)$ by a linear function.[3,4] Let the signal spectrum be given by

$$\tilde{s}(\nu') = f(\nu')\exp[i\varphi(\nu')], \tag{4}$$

where $f(\nu')$ and $\varphi(\nu')$ are real functions that describe the amplitude and the phase of the spectrum, respectively. Consider a narrow spectral window function $G(\nu)$ such that we can use the following approximation:

$$\begin{aligned}\tilde{s}(\nu') &= f(\nu')\exp[i\varphi(\nu')] \\ &\approx f(\nu)\exp\{i[\varphi(\nu) + \dot{\varphi}(\nu)(\nu' - \nu)]\},\end{aligned} \tag{5}$$

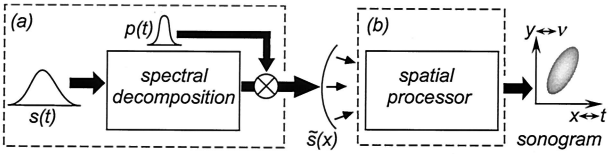

Fig. 1. Schematic representation of the sonogram-generation apparatus. The spectral phase of the input pulse $s(t)$ is converted to the spatial phase of the wave front $\tilde{s}(x)$ by gating of the spectrally decomposed signal with time-domain pulse $p(t)$. A spatial processor generates a sonogram of the input signal that is converted to the spatial domain.

where we use the Taylor expansion about point $\nu' = \nu$ and keep only the first term for the amplitude and first two terms for the phase. Substituting expression (5) into Eq. (2) yields

$$\begin{aligned}W(t, \nu) = |f(\nu)|^2 \Bigg| \int G(\nu - \nu')\exp\{i2\pi[\dot{\varphi}(\nu) \\ /2\pi - t]\nu'\}\mathrm{d}\nu' \Bigg|^2.\end{aligned} \tag{6}$$

For each frequency ν, function $W(t, \nu)$ provides the magnitude of the Fourier transform of window function $G(\nu')$ centered at the coordinate $t = \varphi(\nu)/2\pi$. Therefore one can find group delay $\dot{\varphi}(\nu)$ by determining the position of the center of mass of the sonogram along the t axis. We now find the spectral phase by integrating $\dot{\varphi}(\nu)$:

$$\varphi(\nu) = \int \dot{\varphi}(\nu)\mathrm{d}\nu, \tag{7a}$$

whereas the spectral intensity is found by integration of the sonogram along the time axis, yielding

$$|\tilde{s}(\nu)|^2 \propto \int W(t, \nu)\mathrm{d}t. \tag{7b}$$

Equations (7) characterize the complex amplitude of the ultrashort signal in the frequency domain, and its complex amplitude in the time domain can be found by application of the inverse Fourier transform.

The center-of-mass algorithm described above has proved to be fast and reliable for single-peaked pulses with both linear and nonlinear chirp.[4] However, it becomes ambiguous if the signal consists of several pulses [strictly speaking, if group delay $\dot{\varphi}(\nu)$ is not a single-valued function of ν]. In this case the iterative algorithm introduced in Refs. 5 and 7 and tested for a variety of signals including double pulses can be applied.

3. Description of the Sonogram-Generation Technique

Our method for generating the sonogram of an ultrashort laser pulse is depicted schematically in Fig. 1. The apparatus consists of two optical subsystems, a temporal spectrum processor and a spatial spectrum processor. The key element of the approach is the

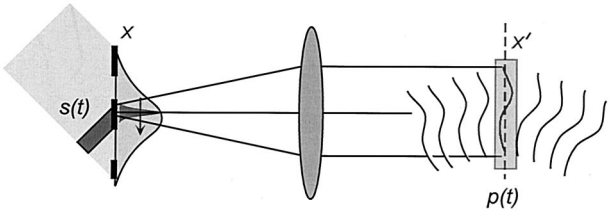

Fig. 2. Setup for spectral decomposition. The solid curves around the back focal plane of the lens illustrate the rotation of the SDW; the part of the wave front sampled by gating pulse $p(t)$ is highlighted with a shaded rectangle.

transformation of the spectral phase of the signal pulse into the spatial phase of a time-gated spectrally decomposed wave (SDW). This transformation is performed in the temporal spectrum processor [Fig. 1(a)]. The spatial phase is then analyzed with the spatial spectrum processor [Fig. 1(b)], producing a two-dimensional image in the spatial domain with its x–y coordinates corresponding to the t–ν coordinates of the ultrafast waveform. In what follows, we describe the principle of operation of these two subsystems.

The temporal spectrum processor (see Fig. 2) uses a standard spectral decomposition device consisting of a diffraction grating in the front focal plane of a lens that is used to perform a spatial Fourier transform. An input ultrashort pulse with complex amplitude $s(t)$ at a carrier frequency ν_0 is transformed into a spectrally decomposed wave in the back focal plane of the lens, yielding[8,9]

$$U_F(t, x') \propto \tilde{s}(ax')\exp(-i2\pi\nu_0 t)\exp(-i2\pi ax't), \tag{8a}$$

where we define the parameter $a = \nu_0/\alpha F$, $\alpha = \sin(\theta)$ is the grating dispersion for incidence angle θ, F is the focal length of the lens, x' is the transverse spatial coordinate in the focal plane of the lens, and $\tilde{s}(ax') = \int s(t)\exp(-i2\pi ax't)\mathrm{d}t$. Substituting Eq. (4) for the complex spectrum $\tilde{s}(ax')$ in relation (8a), we obtain

$$U_F(t, x') \propto f(ax')\exp[i\varphi(ax')] \times \exp(-i2\pi\nu_0 t)\exp(-i2\pi ax't). \tag{8b}$$

Relation (8b) shows that the spectral phase of input ultrashort pulse $\varphi(\nu)$ has been transformed into the spatial phase, $\varphi(ax')$, carried by the SDW. However, further analysis of relation (8b) shows that direct detection of the spatial phase is not possible because of the time-varying linear phase term $\exp(-i2\pi ax't)$. That term can be seen as a rotation of the wave front $\tilde{s}(ax')$ in time, occurring as a consequence of a pulse front tilt, generated by ultrashort pulse scanning across the input pupil of the grating.[9] Ultrafast time gating of the SDW[10] is used to eliminate this effect. A short time-domain gating pulse $p(t)$ is mixed with the SDW in a nonlinear material for sampling of the rotating SDW wave front [i.e., sampling of the linear phase factor $\exp(-i2\pi ax't)$ in relations (8)]. The resultant sampled SDW becomes a short pulse of duration equal to that of the gating pulse; the spatial phase across its transverse aperture is a replica of the spectral phase of the original complex-amplitude ultrafast signal.

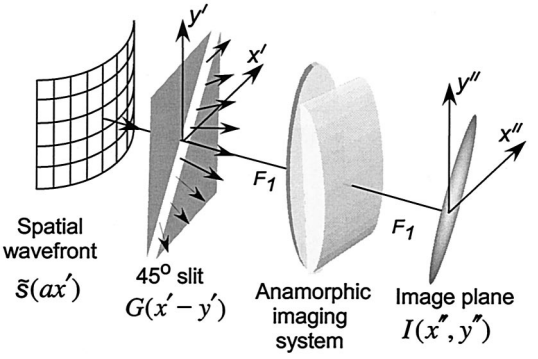

Fig. 3. Spatial sonogram processor. The cylindrical and spherical lenses, both of focal length F_1, are assembled to provide imaging in the y' axis and a Fourier transform in the x' axis.

Next, the time-gated field is introduced into a spatial processor to generate a sonogram of the input ultrashort signal (see Fig. 3).[11] The two-dimensional wave front whose spatial phase varies in the x' direction and is uniform in the y' direction is transmitted through a rectangular slit oriented at 45° relative to the x' axis, yielding filter function $G(\nu)$ in Eq. (1). At each vertical coordinate y' the filter transmits a part of the incident wave front at a coordinate $x' = y'$. An anamorphic imaging lens, consisting of attached spherical and cylindrical lenses with the same focal length F_1, is used for imaging of the filtered SDW field in the y' direction while the Fourier transform is performed in the x' direction. Assuming that the gating pulse is infinitely short (i.e., that it can be approximated by a δ function) and completely eliminates the time-varying linear phase, the intensity distribution in the output image plane yields (see Appendix A)

$$I(x'', y'') \propto \left| \int \tilde{s}(ax')G(x' - y')\exp(-i2\pi bx'x'')\mathrm{d}x' \right|^2, \tag{9}$$

where $b = 2\nu_0/cF_1$. Relation (9) represents a spatial distribution that describes the sonogram of the input temporal signal [as defined by Eq. (2)] mapped to the spatial domain. The validity of approximating gating pulse $p(t)$ by a δ function and the effect of its finite width on the sonogram is further discussed in Section 5 below. Note that, as follows from relation (9), for a high-resolution spectral decomposition device the spectral and temporal resolution in the sonogram is defined not by the resolving power of the spectrometer but by the width of the spatial filter, $G(x' - y')$.

4. Experimental Results

For experimental evaluation of the technique described above we use ultrashort pulses from a commer-

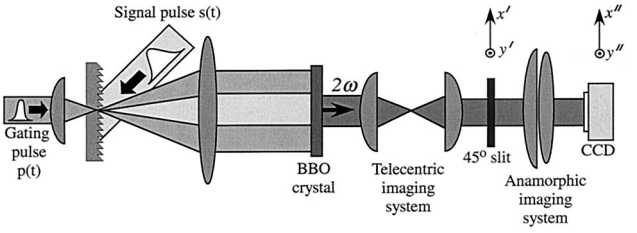

Fig. 4. Experimental setup. The spectrally decomposed signal pulse (Fig. 2) is mixed with the gating pulse in a 0.25-mm-thick BBO crystal, generating a sum-frequency field whose spatial phase is a replica of the spectral phase of the signal.

cial Ti:sapphire oscillator, producing 100-fs pulses at a wavelength of 800 nm with an energy of 7 nJ. The laser output is split into a signal pulse and a gating pulse, with ~20% and ~80% of the total power, respectively. The spectral decomposition device is implemented by a 600-line/mm grating combined with a 150-mm focal-length spherical lens. Both the SDW and the gating pulse are focused in the y' direction (i.e., along the axis perpendicular to the direction of spectral decomposition) onto a 0.25-mm-thick β-barium borate (BBO) crystal, generating a sum-frequency signal in type I phase-matching geometry (see Fig. 4). The output crystal plane is telecentrically imaged onto the 45° spatial filter by a pair of cylindrical lenses that image in x' direction while they allow free-space propagation of the field in the y' direction. Focusing the beams into the nonlinear medium increases the conversion efficiency of the nonlinear process, whereas free-space propagation in the y' direction after the crystal is used to expand the spatial mode for subsequent spatial filtering (Fig. 3). To provide undistorted spectral intensity information, the spatial mode of the sum-frequency field generated in the y' direction should be constant across the spatial filter aperture. This can be achieved by appropriate expansion of the mode. However, instead, we found it beneficial to make an independent measurement of the spectral intensity, such that we could use the entire spatial mode of the generated sum-frequency signal and thus improve the signal-to-noise ratio for measurement of the phase (which is not affected by the nonuniform spatial mode). One can easily integrate the spectral intensity measurement into our single-shot arrangement by simply splitting a small fraction of the spectrally decomposed signal and introducing it onto a linear detector array. Alternatively, one could measure the spatial distribution of the sum-frequency field across the y' axis and incorporate a corresponding correction factor within the reconstruction procedure.

Figure 5 shows the experimental results obtained with the ultrashort signal derived from the output of the laser oscillator (top) and for the pulse chirped by a grating pair (bottom). As expected, a nearly transform-limited pulse generated by the mode-

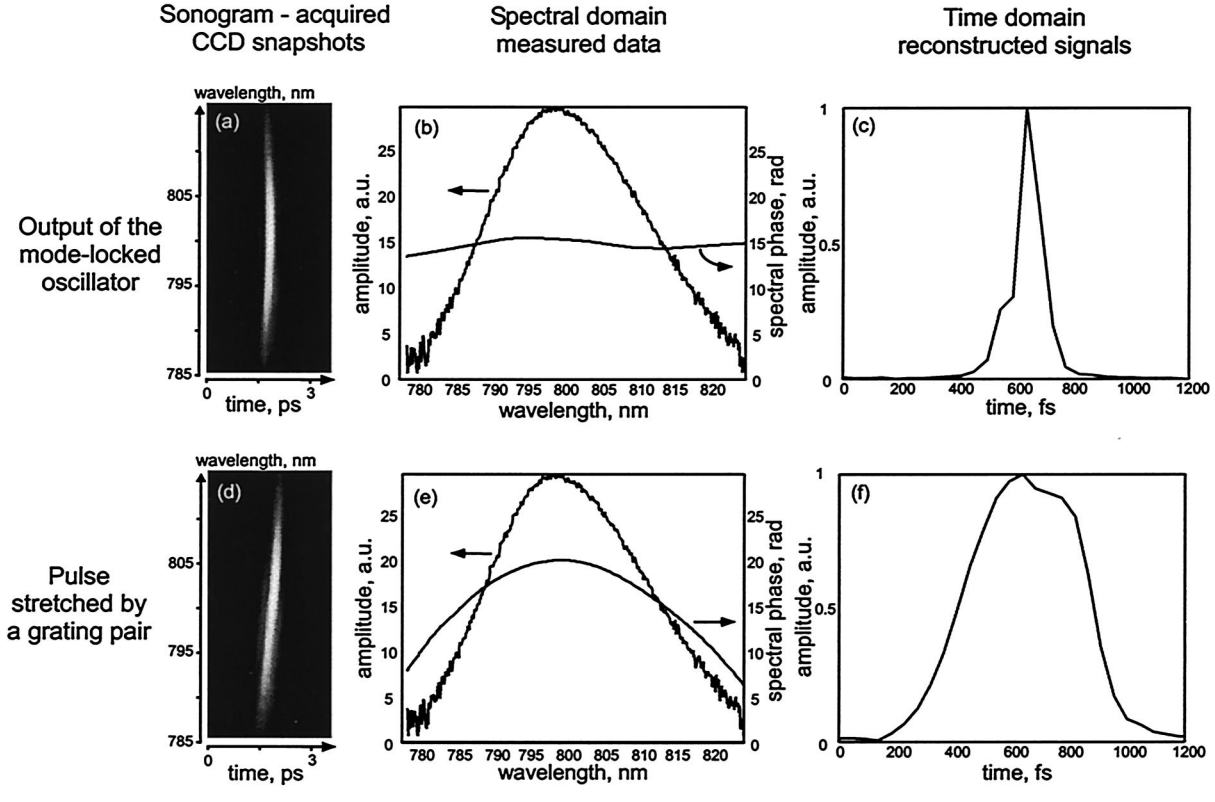

Fig. 5. Experimental results for the mode-locked oscillator pulses. Top, results for the pulse from the output of the oscillator: (a) sonogram snapshot, (b) spectral phase and amplitude, and (c) reconstructed time-domain signal profile. Bottom, results for the pulse stretched by a grating pair: (d) sonogram snapshot, (e) spectral phase and amplitude, and (f) reconstructed time-domain signal profile.

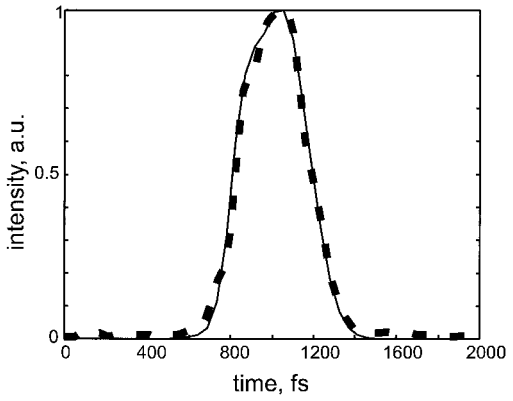

Fig. 6. Comparison of the measured (dashed curve) cross correlation between signal pulses used to generate the sonograms of Figs. 5(a) and 5(c) and the cross correlation generated numerically from the reconstructed pulses of Figs. 5(c) and 5(f) (solid curve).

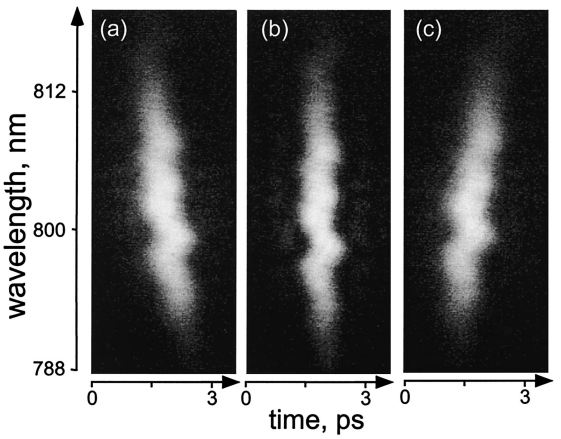

Fig. 7. Sonogram snapshots illustrating the optimization of the compressor of the regenerative amplifier: (a) positively chirped, (b) compressed, (c) negatively chirped pulses.

locked oscillator produces a time-gated SDW with a constant phase wave front and has a sonogram described by a vertical line. In contrast, linear chirp causes a rotation of the sonogram, indicating the existence of the quadratic phase. To verify the validity of our technique we used a femtosecond pulse imager[9] to measure the intensity cross correlation between two signal pulses that were used to generate the sonograms in Figs. 5(a) and 5(d). Using reconstructed temporal profiles of Figs. 5(c) and 5(f), we generated the cross-correlation function numerically and compared it with the experimentally measured function. Figure 6 shows excellent agreement of the two independent results.

5. Discussion: Effect of Finite Length of the Gating Pulse

In deriving Relation (9) we assumed the gating pulse to be infinitely short and therefore completely eliminated the SDW rotation in time (Fig. 2). The finite temporal width of the gating pulse results in convolution of the true sonogram of relation (9) and the temporal intensity profile of gating pulse $p(t)$:

$$I'(x'', y'') \propto \int |p(t)|^2 I[x'' + (a/b)t, y'']\mathrm{d}t, \quad (10)$$

where we defer the derivation of relation (10) to Appendix A. The convolution effect caused by the finite pulse width of the gating pulse is not intrinsic to our method; a similar effect occurs in other sonogram measurement techniques.[7] Relation (10) sets the criteria for validity of approximating gating pulse $p(t)$ with a δ function. As can be seen from Eq. (6), the width of the sonogram distribution in the x' direction is determined by the width of the Fourier transform of the filter function, $\tilde{G} = \mathrm{F.T.}\{G\}$. Therefore if the gating pulse width is sufficiently narrow relative to the width of $\tilde{G}$, the δ-function approximation is valid. Because the width of filter function G is at least several times smaller than the bandwidth of the signal under test, $\Delta\nu$, the width of $\tilde{G}$ will be always larger than $1/\Delta\nu$. Therefore the δ-function validity condition will hold for pulses that do not possess large time–bandwidth products $\Delta\nu\Delta t$ (i.e., for the pulses that are not heavily chirped).

To account for the distortion of the signal described by relation (10), a modified iterative algorithm has been proposed.[7] However, for single-pulse signals the effect of the convolution operation will result only in broadening of the sonogram distribution in time. The spectral phase can still be extracted by use of the center-of-mass method, while the distorted sonogram of Eq. (6) provides a useful illustration of the signal features.

To demonstrate the capability of operating with a broad gating pulse we used the output of a regenerative optical amplifier to derive both the signal and the gating pulses. We observed in real time the sonogram of the amplifier pulses and used it to optimize the separation between the pair of gratings that was used in the amplifier to generate a compressed output pulse. Figure 7 illustrates the transformation of the sonogram as the pulse is adjusted from positively chirped to compressed to negatively chirped. The wiggling of the sonogram manifests the existence of nonlinear chirp, which results in the background and ripples on the trailing edge of

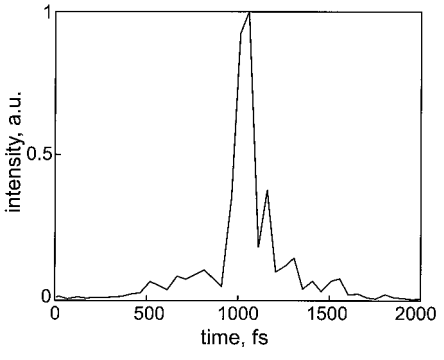

Fig. 8. Temporal profile of the pulse from the regenerative amplifier for optimum compressor grating separation [corresponds to the sonogram shown in Fig. 7(b)].

the temporal profile of the pulse reconstructed from the sonogram of Fig. 7(b) (see Fig. 8). One can observe a decrease in the time resolution in Figs. 7(a) and 7(c) as the gating pulse is stretched to be ~8 times wider than the compressed pulse (~800 fs). Although the resolution is decreased, the sonogram trace is intuitive, providing real-time information about the analyzed signal.

6. Conclusion

In summary, we have introduced a technique for single-shot generation of the sonogram of an ultrashort laser pulse. The method uses time gating of the spectrally decomposed field of the test pulse to transfer its spectral phase into the spatial phase of the time-gated spectrally decomposed wave. A spatial filtering of the time-gated field produces the sonogram, which is analyzed to provide the spectral phase and amplitude of the test pulse. The method was demonstrated experimentally with femtosecond laser pulses that possessed both linear and nonlinear chirp. Independent measurement of the pulse width showed excellent agreement with the data obtained from the sonogram, proving that our apparatus is a reliable tool for characterization of ultrashort pulses. The effect of broadening of the gating pulse was analyzed. Like other sonogram-generation techniques with broad gating pulses, the method produces a distorted sonogram. However, we have demonstrated that practically for a single-peaked test pulse the apparatus is able to tolerate significant broadening of the gating pulse.

Appendix A: Effect of the Temporal Width of the Gating Pulse on the Sonogram

Here we derive relations (9) and (10), demonstrating the effect of the gating pulse on the detected signal. Under the assumptions of small conversion efficiency and perfect phase matching, sum-frequency field U_{sum}, generated in the process of time gating of the SDW U_F [relation 8(a)], can be represented as

$$\begin{aligned} U_{\mathrm{sum}} &\propto U_F p(t)\exp(-i2\pi\nu_0 t) \\ &= p(t)\tilde{s}(ax')\exp[-i2\pi(2\nu_0 + ax')t]. \end{aligned} \tag{A1}$$

The sum-frequency field is transmitted through the spatial filter with transmittance $G(x' - y')$ and is processed by an anamorphic lens, performing a Fourier transform and imaging in the x' and y' directions, respectively (Fig. 3). The resultant signal intensity I is detected by a CCD, which also performs the time integration

$$\begin{aligned} I(x'', y'') = \int \Bigg| \int\int U_{\mathrm{sum}}(x', t)G(x' - y') \\ \times \exp(-i2\pi bx'x'')\delta(y' - y'')\mathrm{d}y'\mathrm{d}x' \Bigg|^2 \mathrm{d}t, \end{aligned} \tag{A2}$$

where x'' and y'' are transverse coordinates in the detection plane and a spatial δ function describes the imaging process. Substituting relation (A1) into Eq. (A2) and integrating over y' yield the desired result:

$$\begin{aligned} I(x'', y'') = \int \mathrm{d}t|p(t)|^2 \Bigg| \int \tilde{s}(ax')G(x' \\ - y'')\exp\{-i2\pi x'b[x'' + (a/b)t]\}\mathrm{d}x' \Bigg|^2. \end{aligned} \tag{A3}$$

If the δ-function approximation for the gating pulse is valid, integration in time yields relation (9).

This research was supported by the National Science Foundation, the U.S. Air Force Office of Scientific Research, Applied Micro Circuits Corporation, and the Defense Advanced Research Projects Agency. D. Panasenko gratefully acknowledges the support of the Fannie and John Hertz Foundation.

References

1. D. J. Kane and R. Trebino, "Single-shot measurement of the intensity and phase of an arbitrary ultrashort pulse by using frequency-resolved optical gating," Opt. Lett. **18,** 823–825 (1993).
2. K. W. DeLong, R. Trebino, J. Hunter, and W. E. White, "Frequency-resolved optical gating with the use of second-harmonic generation," J. Opt. Soc. Am. B **11,** 2206–2215 (1994).
3. J. L. A. Chilla and O. E. Martinez, "Direct determination of the amplitude and the phase of femtosecond light pulses," Opt. Lett. **16,** 39–41 (1991).
4. J.-K. Rhee, T. S. Sosnowski, A.-C. Tien, and T. B. Norris, "Real-time dispersion analyzer of femtosecond laser pulses with use of a spectrally and temporally resolved upconversion technique," J. Opt. Soc. Am. B **13,** 1780–1785 (1996).
5. V. Wong and I. A. Walmsley, "Ultrashort pulse characterization from dynamic spectrograms by iterative phase retrieval," J. Opt. Soc. Am. B **14,** 944–949 (1997).
6. K. W. DeLong, R. Trebino, D. N. Fittinghoff, and C. L. Ladera, "Review of time-frequency domain concepts with application to ultrashort laser pulses," in *Generation, Amplification, and Measurement of Ultrashort Laser Pulses II*, C. P. Barty and F. W. Wise, eds., Proc. SPIE **2377,** 44–51 (1995).
7. D. T. Reid, "Algorithm for complete and rapid retrieval of ultrashort pulse amplitude and phase from a sonogram," IEEE J. Quantum Electron. **35,** 1584–1599 (1999).
8. M. B. Danailov and I. P. Christov, "Time–space shaping of light pulses by Fourier optical processing," J. Mod. Opt. **36,** 725–731 (1989).
9. P.-C. Sun, Y. T. Mazurenko, and Y. Fainman, "Femtosecond pulse imaging: ultrafast optical oscilloscope," J. Opt. Soc. Am. A **14,** 1159–1170 (1997).
10. K. Ema, M. Kuwata-Gonokami, and F. Shimizu, "All-optical sub-Tbits/s serial-to-parallel conversion using excitonic giant nonlinearity," Appl. Phys. Lett. **59,** 2799–2801 (1991).
11. H. O. Bartelt, K.-H. Brenner, and A. W. Lohmann, "The Wigner distribution function and its optical production," Opt. Commun. **32,** 32–38 (1980).